Correlation spectroscopy in cold atoms: Light sideband resonances in electromagnetically-induced-transparency condition

H. M. Florez, A. Kumar, K. Theophilo, P. Nussenzveig, and M. Martinelli*
Instituto de Física, Universidade de São Paulo, 05315-970 São Paulo, SP-Brazil
(Received 31 March 2016; published 6 July 2016)

The correlation spectroscopy has been successfully employed in the measurement of the intrinsic linewidth of electromagnetically induced transparency (EIT) in time and frequency domain. We study the role of the sidebands of the intense fields in the measured spectra, analyzing the information that can be recovered working with different analysis frequencies. In this case, the nonzero one-photon detuning appears as a necessary condition for spectrally resolving the sideband resonances in the correlation coefficient. Our experimental findings are supported by the perturbative model defined in the frequency domain.

DOI: 10.1103/PhysRevA.94.012504

One of the widely used mechanisms that provide coherent mapping between light and matter is electromagnetically induced transparency (EIT) [1–3]. Such light-matter interface finds applications in quantum memories and quantum repeaters [4–6]. It can also be employed for quantum nondemolition measurements [7] and as a source of intense quantum correlated light beams [8,9].

Recently, it was shown that the correlation spectroscopy can be used as a technique for measuring the intrinsic linewidth of the EIT resonance [10–12], which is directly related to the decoherence lifetime of the involved ground states. This linewidth is narrower than the broadened EIT linewidth usually measured by the standard transmission spectroscopy. Therefore, it was shown to be a useful spectroscopic tool to estimate the decoherence limitations in quantum memories protocols based on EIT. These intensity correlation techniques could also be of interest in precision measurements in atomic clocks relying on coherent population trapping [13].

Different research groups have been investigating how intensity correlation of two fields is affected by a medium, with special interest in the EIT process. Noise spectroscopy has shown to be a powerful method for this investigation [14]. The analysis of the intensity correlation can be done either in time [11,15,16] or in frequency domains [9,10,12,17–19] using, respectively, the $g^{(2)}(\tau)$ function or its Fourier transform $C(\omega)$.

Felinto *et al.* [11] proposed a heuristic model for $g^{(2)}(0)$, and applied it to cold-atomic systems where Doppler broadening is negligible. It was demonstrated that correlation noise spectroscopy is power broadening free in this case, and that the linewidth of the $g^{(2)}(0)$ function is determined by the ground-state decoherence lifetime.

In the frequency domain, the power broadening free features of the intrinsic EIT linewidth have been shown in a study of intensity correlation spectra $C(\omega)$ obtained with cold alkali-metal atoms (rubidium and cesium) [12], with the advantage that with proper selection of analysis frequency the contribution from electronic noise to the measurement is either negligible or can be easily subtracted. Moreover, with the recent developments of quantum optics in frequency domain (especially multimode quantum optics [20], and the observation of multimode coherent effects [21]) stimulates the investigation of the atomic behavior in similar situations.

Careful study of correlations in frequency domain shows the contributions from the sidebands of the main field [22]. While they do not affect the narrow structure related to the intrinsic linewidth, the whole profile of the correlation inside the typical EIT linewidth is broadened by the sideband resonances, a major difference between analysis in time [11] and frequency [12] domains.

In this work, we explore the role of the sideband resonances and the effect of the detuning in the correlation profile. We show that the interplay between one-photon detuning and analysis frequency ω opens the possibility of detecting atomic response to sidebands in correlation spectra. We also show that in such condition the correlation linewidth measured in the frequency domain is exactly the same as the one in the time domain for the $g^2(0)$ described in [11]. Moreover, it is shown experimentally that when one of the beams is kept in resonance with the atomic transition, independent correlation information of the sidebands and the carriers is unavailable [22], therefore demonstrating the richer structure contained in $C(\omega)$ in comparison with $g^2(0)$.

In addition, the perturbative method we use provides a physical insight on the mapping of the atomic response with the correlation functions $g^{(2)}(0)$ and $C(\omega)$. Unlike the resonant case, where the dispersive response seems responsible for the main contribution in the intensity correlation, in the nonresonant case there is a balance between the absorptive and dispersive response. Such a balance makes the heuristic model for $g^{(2)}(0)$ a valid approximation of $C(\omega)$ only inside the typical EIT linewidth, failing at higher two-photon detunings.

Our presentation is organized as follows. In Sec. I, we briefly describe the technique of correlation spectroscopy and the level scheme used in our study. We also describe the theoretical model used to define the correlation coefficient in frequency domain. In Sec. II, we discuss the details of our experiment, starting from a cold cloud of ^{87}Rb, and present the control of the involved parameters. In Sec. III, we show the results of correlation spectroscopy with different values of one-photon detuning, and compare it to the theory. We also show how the presence of the sidebands is revealed in the correlation spectrum obtained at different one-photon detunings. In Sec. IV, we discuss our results and in Sec. V we summarize our findings of correlation spectroscopy done at different values of one-photon detuning.

*mmartine@if.usp.br

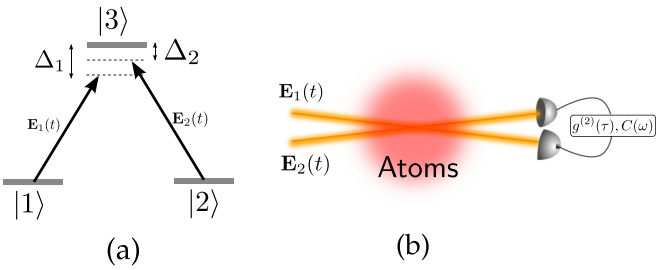

FIG. 1. (a) Levels scheme in Λ-type configuration for EIT. (b) Basic setup for measuring the intensity correlation spectra in time $[g^{(2)}(\tau)]$ or frequency domain $[C(\omega)]$.

I. THEORY: CORRELATION SPECTROSCOPY

Inspired in the Hanbury-Brown and Twiss's experiments, the intensity correlation between two light fields with intensities $I_1(t)$ and $I_2(t+\tau)$ can be quantified by the $g^{(2)}(\tau)$ function [15].

Our interest is to analyze such intensity correlation between two light fields induced by cold-atomic media in the EIT condition. Yabuzaki *et al.* [14] showed that the atomic medium converts excess phase noise of the input light sources into intensity noise at the output field. Therefore, to model the intensity correlation induced by the atoms in our bipartite system, the transformation of phase noise to amplitude noise has to be considered.

Our scheme for correlation spectroscopy in a Λ-EIT condition is shown in Fig. 1(a). Two fields $\mathbf{E}_1(t)$ and $\mathbf{E}_2(t)$ are coupled to two different transitions of a three-level atom, with different one-photon detunings Δ_1 and Δ_2, respectively. The intensity correlation between the two fields is measured after interacting with the atomic ensemble as presented in Fig. 1(b). The previously reported correlation spectroscopy [10–12,23] has been done by setting one of the fields in resonance (e.g., $\Delta_1 = 0$), while scanning the detuning of the second field around the resonance. However, in this work, we set different values of detuning Δ_1, i.e., $\Delta_1 \neq 0$ while Δ_2 is scanned around Δ_1.

In what follows, we present a brief description of the semiclassical approach for the intensity correlation spectrum based on the conversion of phase noise to amplitude noise. We consider two electromagnetic fields described by

$$\mathbf{E}_i(t) = \mathcal{E}_i \exp\left[i(\omega_i t + \phi_i(t))\right]\mathbf{e}_i, \tag{1}$$

with a stochastic phase fluctuation ϕ_i that models the excess of noise in diode lasers. In the expression for the fields, $i = 1,2$ denotes the two beams, $\mathcal{E}_i$ and ω_i are, respectively, the amplitude and the frequency of each beam.

Photodetectors are not sensitive to the phase noise of light beams. However, the interaction of light fields through an atomic medium makes it detectable by mapping the phase noise into amplitude noise (PN-AN). Under the thin sample limit [24], the field after propagation through atomic media is given by $\mathbf{E}_i^{\text{out}}(t) = \mathbf{E}_i(t) + i\kappa\mathbf{P}_i(t)$, where polarization $\mathbf{P}_i(t)$ represents the atomic response induced by the incident fields $\mathbf{E}_i(t)$ and κ_i is a real constant that depends on the atomic density. The induced polarization term is responsible for transforming the phase noise ϕ_i [contained in $\mathbf{E}_i(t)$] into amplitude noise detected in $\mathbf{E}_i^{\text{out}}(t)$. In a Λ-EIT configuration [Fig. 1(a)], the polarization induced in atomic medium by two incident fields can be given as $\mathbf{P}_i = \mathbf{d}_{i3}\rho_{i3}$, where $\mathbf{d}_{i3}$ and ρ_{i3} represent the electric dipole moment and the atomic coherence associated to the fields $i = 1,2$. The output intensity of the beam is given by $I_i^{\text{out}}(t) = |\mathbf{E}_i^{\text{out}}(t)|^2$.

In order to describe the correlation between two intense light beams, we average correlations of the fluctuations in both beams $\delta I_i(t) = I_i^{\text{out}}(t) - \langle I_i^{\text{out}}\rangle$ with $i = \{1,2\}$ for different instants of time separated by τ. There are two possible approaches to calculate the intensity correlation: in the time-domain approach adopted in [10,11,16,17], the intensity correlation between two light fields can be easily described in terms of the atomic variables as [11]

$$\begin{aligned} g^{(2)}(0) &= \frac{\langle \delta I_1(t)\delta I_2(t)\rangle}{\sqrt{\langle \delta^2 I_1(t)\rangle\langle \delta^2 I_2(t)\rangle}} \\ &= \frac{\text{Re}p_1\text{Re}p_2 + \text{Im}p_1\text{Im}p_2}{\sqrt{(\text{Re}^2 p_1 + \text{Im}^2 p_1)(\text{Re}^2 p_2 + \text{Im}^2 p_2)}}, \end{aligned} \tag{2}$$

where polarization terms are related to atomic coherences as $p_i = \rho_{i3}^{ss}$ and the notations $\text{Im}^2 p_i = (\text{Im}p_i)^2$ and $\text{Re}^2 p_i = (\text{Re}p_i)^2$. The ss index stands for steady state. The atomic response induces correlation $[g^{(2)}(0) > 0]$ or anticorrelation $[g^{(2)}(0) < 0]$ between the light fields, depending on two-photon detuning $\delta = \Delta_2 - \Delta_1$ [10,16,17]. At low-power regime, absorption dominates and the medium induces correlation between the light fields. However, as the power of the beams is increased, the dispersion term $\text{Re}\langle p_1\rangle\text{Re}\langle p_2\rangle < 0$ overcomes the contribution from the absorption term $\text{Im}\langle p_1\rangle\text{Im}\langle p_2\rangle > 0$, leading to anticorrelated light fields.

Another possible approach is the analysis of intensity fluctuations $\delta I_i(t+\tau)$ in their different spectral components by a Fourier transform. Therefore, the correlation in the frequency domain description is defined as

$$C(\omega) = \frac{S_{12}(\omega)}{\sqrt{S_{11}(\omega)S_{22}(\omega)}}, \tag{3}$$

where $S_{ij}(\omega)$ represents the symmetrical intensity correlation spectrum for i and j fields at a given analysis frequency ω such that

$$\begin{aligned} S_{ij}(\omega) = \frac{1}{4\pi}\int_{-\infty}^{\infty} d\tau\, e^{-i\omega\tau}[&\langle \delta I_i(t)\delta I_j(t+\tau)\rangle \\ &+ \langle \delta I_j(t)\delta I_i(t+\tau)\rangle]. \end{aligned} \tag{4}$$

Similar to $g^{(2)}(0)$, the function $C(\omega)$ is also normalized such that for correlated fields $1 \geqslant C(\omega) > 0$, and for anticorrelated fields $-1 \leqslant C(\omega) < 0$.

A perturbative approach is proposed in Ref. [22] to describe the correlation coefficient of Eq. (3) in terms of the absorption and dispersion of the fields, similar to the case of $g^{(2)}(0)$ function in Eq. (2). Taking the laser linewidth γ as perturbative parameter $\epsilon = \sqrt{\gamma}$ in the expansion of the spectral components of the fluctuations, we can obtain a direct expression for the correlation $C(\omega)$, at the lowest order. The resulting expression

$$C(\omega) = \frac{\nu_{\text{Im}}(\omega)\tilde{\Pi}_{\text{Im}} + \nu_{\text{Re}}(\omega)\tilde{\Pi}_{\text{Re}} + C_{\text{cross}}(\omega) + C_{1|2}(\omega)}{\sqrt{S_{11}(\omega)S_{22}(\omega)}}, \tag{5}$$

where the absorptive, dispersive, and cross terms are, respectively, defined by the polarization terms associated with the atomic coherences

$$\tilde{\Pi}_{\mathrm{Im}} = 2\epsilon^2 \mathrm{Im}p_1 \mathrm{Im}p_2 + O(\epsilon^4), \tag{6a}$$

$$\tilde{\Pi}_{\mathrm{Re}} = 2\epsilon^2 \mathrm{Re}p_1 \mathrm{Re}p_2 + O(\epsilon^4), \tag{6b}$$

$$C_{\mathrm{cross}}(\omega) = \nu_{RI}(\omega)[-2\epsilon^2 \mathrm{Im}p_1 \mathrm{Re}p_2 + O(\epsilon^4)] + \nu_{IR}(\omega)[-2\epsilon^2 \mathrm{Im}p_2 \mathrm{Re}p_1 + O(\epsilon^4)] \tag{6c}$$

$$= \nu_{RI}(\omega)\tilde{\Pi}_{RI}(\omega) + \nu_{IR}(\omega)\tilde{\Pi}_{IR}(\omega), \tag{6d}$$

$$C_{1|2}(\omega) = \chi_{11}(\omega) + \chi_{22}(\omega). \tag{6e}$$

Three main differences will show up when we compare $C(\omega)$ [Eq. (5)] with $g^{(2)}(0)$ [Eq. (2)]. One is the presence of a cross term C_{cross} involving the product of dispersive and absorptive contributions, which is absent in $g^{(2)}(0)$. The second is the need of weighting coefficients $\nu_{\mathrm{Im}}(\omega)$, $\nu_{\mathrm{Re}}(\omega)$, and $\nu_{RI}(\omega)$ [$\nu_{IR}(\omega)$] distorting the main contributions for the correlation (absorption, dispersion, and Stokes transitions, respectively) with a dependence on the analysis frequency ω. The third is the complementary term $C_{1|2}$ which depends on the individual response to each field χ_{11} and χ_{22}. A description of the calculation, as well as the definition for the complementary term $C_{1|2}$, and the explicit expressions for $S_{11}(\omega)$ and $S_{22}(\omega)$ are given in the Appendix A.

Thanks to this perturbative approach, we will understand the observed anticorrelation for $|\delta| > \Gamma$ when $\Delta_1 = 0$ as a consequence of dispersion overcoming absorption. Such situation is very different from the behavior of $g^{(2)}(0)$ functions where the absorptive and dispersive properties contribute equally to the correlation [11]. It can also be understood the role of the mixing of sideband resonances in the PN-AN conversion when the carrier frequency $|\delta| < \Gamma$. This approach is an interesting resource for identifying the necessary conditions to obtain sideband resonances independent from the carriers PN-AN mechanism near the two-photon resonance.

II. EXPERIMENT

We used an ensemble of cold atoms of ^{87}Rb released from a magneto-optical trap (MOT). Diode lasers in $5S_{1/2}(F = 2) \leftrightarrow 5P_{3/2}(F' = 3)$ transition were used for cooling the atoms. Our atomic cloud has nearly 10^7 atoms at 800 μK. Doppler broadening will be limited to 1.5 MHz for each beam, below the atomic linewidth of 6 MHz. Moreover, the EIT process in this nearly copropagating configuration is not sensitive to Doppler broadening. The optical depth of the cloud in the cooling transition is $\sim$1. The Λ-type three-level system considered in the experiment is shown in Fig. 2(a). The correlation spectroscopy is done in the transition $F_G = 5S_{1/2}(F = 1) \rightarrow F_E = 5P_{3/2}(F' = 1)$ where the two fields with orthogonal polarizations $\sigma\mp$ couple the Zeeman levels $m = \pm 1$, respectively, as shown in Fig. 2(a). To bring the atomic population to $5S_{1/2}(F = 1)$, we used an additional optical light-field coupling $5S_{1/2}(F = 2) \rightarrow 5P_{3/2}(F' = 2)$ transition. Moreover, the proposed atomic transitions obey the necessary condition $F_G \geqslant F_E$ for having destructive interference for both atomic coherences of the Λ system, observing EIT in the atomic medium. The opposite condition

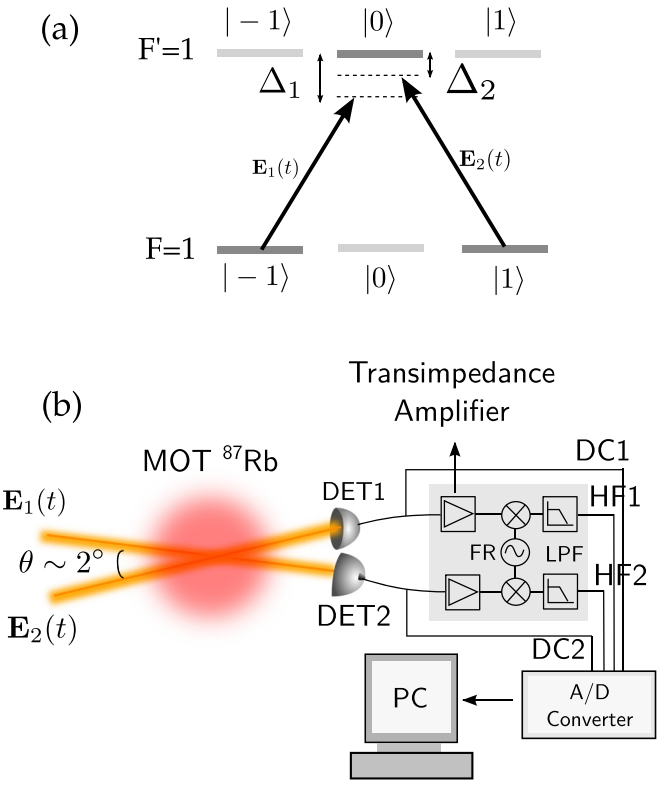

FIG. 2. (a) Level scheme in Λ-type configuration for EIT, detunings Δ_1 (fixed) and Δ_2 (scanned around Δ_1). (b) Basic setup for EIT spectroscopy in cold atoms, where dc and HF signals are detected separately for each beam.

$F_G < F_E$ produces constructive interference and would lead to electromagnetically induced absorption (EIA), as it was demonstrated in Ref. [25].

The two beams with orthogonal polarization components come from the same external cavity diode laser. Although the laser has a linewidth of $\sim$1 MHz (consistent with the stochastic phase noise), the fields are phase correlated to the limit of the standard quantum level (SQL). Each light beam is switched and frequency controlled by independent acousto-optical modulators (AOM) in double-pass configuration. The frequency detuning of each beam is controlled by a computer-controlled digital-to-analog interface acting on the AOM drivers through voltage-controlled oscillators. The optical power for each beam was $P_1 = 112(1)$ μW and $P_2 = 107(1)$ μW, with spot sizes of $w_1 = 1.8(4)$ mm and $w_2 = 1.6(4)$ mm, respectively (with w as the spot radius at $1/e^2$ intensity level of a Gaussian beam). Therefore, the beams are below saturation, with $I_1/I_{\mathrm{sat}} = 0.18$ and $I_2/I_{\mathrm{sat}} = 0.22$. As shown in Fig. 2(b) (not to scale), the two light beams interact with the atomic ensemble at an angle of $\sim 2^\circ$ to avoid any leakage from one beam to another in the detection process.

We used *p-i-n* photodetectors where the photocurrent signals are divided into a dc signal and a high-frequency (HF) signal that is connected to a transimpedance amplifier. Both the signals are sent to an analog-to-digital converter and the data are acquired in a computer. The intensity noise correlation is measured from the HF signal of both detectors. The time sequence for synchronizing the MOT, the probe

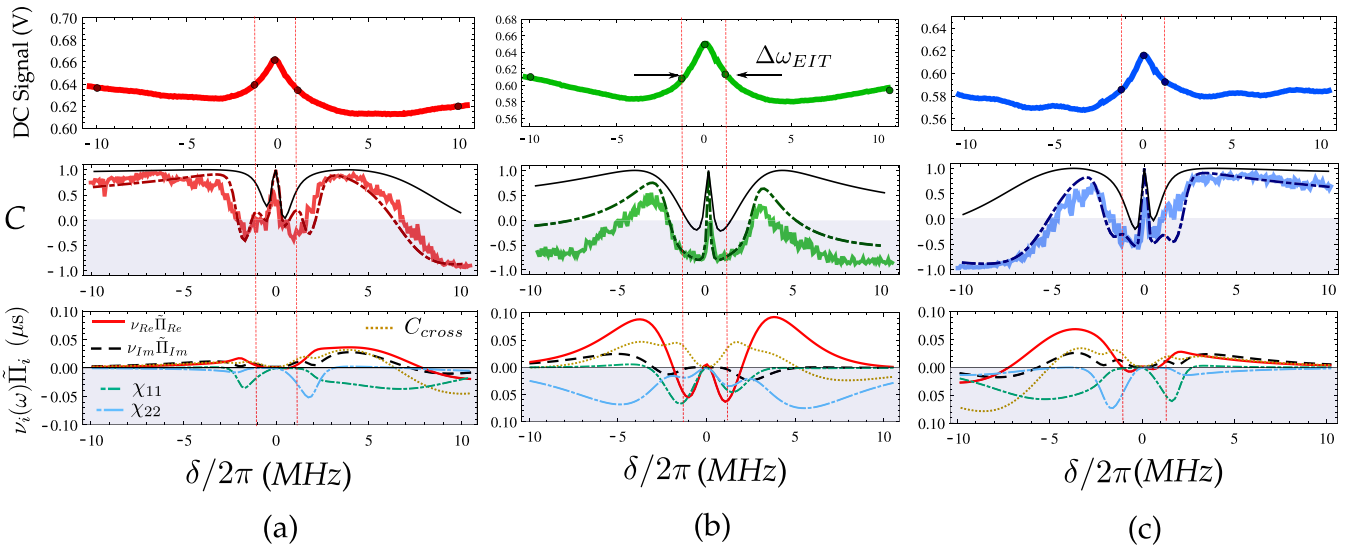

FIG. 3. Spectroscopic results with three different features: dc signal (first row), correlation (second row), and the decomposition terms $\nu(\omega)_i\tilde{\Pi}_i$ of Eq. (5) of the perturbative treatment (third row). Spectroscopy for (a) detuned case $\Delta_1/2\pi = -6$ MHz, (b) resonant case $\Delta_1 = 0$ MHz, and (c) detuned case $\Delta_1/2\pi = 5$ MHz. The experimental correlation spectra in (a), (b), and (c) are shown in solid thick lines. The perturbative result for $C(\omega)$ and heuristic model for $g^{(2)}(0)$ are traced in dotted-dashed and solid thin lines, respectively (second row). The parameters used for the atomic medium are as follows: decoherence rate $\gamma_d/2\pi = 150$ kHz, analysis frequency $\omega/2\pi = 2$ MHz, phase noise $\gamma/2\pi = 1$ MHz. The Rabi frequencies corresponding to the experimental values of intensity are $\Omega_1 = 0.30\,\Gamma$ and $\Omega_2 = 0.34\,\Gamma$. The one-photon detunings used for the theoretical spectra are $\Delta_1/2\pi = -6$, 0.2, and 5 MHz, respectively, from left to right.

beams for spectroscopy, and the detection scheme is the same as described in Ref. [12]. The spectroscopy is performed in 0.5 ms while scanning the detuning of beam 2, detuning of beam 1 is kept at a fixed value, and all presented spectra are averaged over 100 scans.

III. RESULTS

In Fig. 3, we show the spectroscopic results for three different values of one-photon detuning $\Delta_1/2\pi$: -6 MHz (a), 0 MHz (b), and 5 MHz (c). Each row in Fig. 3 represents different features. The top row presents the dc signal, which measures the transmission of the beams and is associated with the mean value of the photocurrent. The second row presents the correlation function $C(\omega)$ for an analysis frequency $\omega/2\pi = 2$ MHz. The third and fourth rows show the calculated values of the main $\tilde{\Pi}$ elements and their respective weighted values $\nu(\omega)$ multiplied by $\tilde{\Pi}$ elements, as introduced in Eqs. (5) and (6). All the curves are plotted as a function of the two-photon detuning $\delta = \Delta_2 - \Delta_1$. In all curves, the dashed vertical lines shows the EIT linewidth of 2.5 MHz, experimentally obtained from the dc signal.

Let us first discuss the resonant case, i.e., $\Delta_1 = 0$, shown in Fig. 3(b). In this case, we observe a typical EIT profile in the dc signal, which allows the measurement of a linewidth $\Delta\omega_{\rm EIT}$ from the full width at half maximum of the peak. As for the correlation $C(\omega)$, we notice that the two fields are anticorrelated for $|\delta|/2\pi > 5$ MHz and also for $|\delta|/2\pi < 2$ MHz, with a narrow correlated peak at exact two-photon resonance. As it was discussed in [11,12], this narrow structure is insensitive to power broadening and can be associated to the coherence between the ground states. The $g^{(2)}(0)$ function from the heuristic model in Eq. (2) is also plotted in solid thin line. Although it presents a similar shape, the result is mostly correlated, with anticorrelation only for $|\delta|/2\pi \sim 1$ MHz. This is a consequence of the combination of $\mathrm{Im}p_1\mathrm{Im}p_1$ and $\mathrm{Re}p_1\mathrm{Re}p_1$ given in Eq. (2) [11], where for most of the detunings the absorptive (positive) term dominates over the dispersive (negative) term.

In order to understand the observed anticorrelation that rises in the frequency domain, we should refer to the terms contributing to Eq. (5). Looking at the values of $\nu_i(\omega)\tilde{\Pi}_i$ in the EIT region $|\delta| \lesssim \Delta\omega_{\rm EIT}$, we can observe the low absorptive contribution $[\nu_{\rm Im}(\omega)\tilde{\Pi}_{\rm Im}]$ compared to the dispersive term $\nu_{\rm Re}(\omega)\tilde{\Pi}_{\rm Re}$. In fact, there is a competition among the dispersive term $[\nu_{\rm Re}(\omega)\tilde{\Pi}_{\rm Re}]$, the cross terms $[C_{\rm cross}(\omega)]$, and the individual terms $\chi_{11}(\omega)$ and $\chi_{22}(\omega)$ that accounts for the resultant anticorrelated value. For $\delta/2\pi > 5$ MHz, the absorptive term $\nu_{\rm Im}(\omega)\tilde{\Pi}_{\rm Im}$ is negligible while the positive contribution of the dispersive term $\nu_{\rm Re}(\omega)\tilde{\Pi}_{\rm Re}$ is highly compensated by the terms $\chi_{11}(\omega)$ and $\chi_{22}(\omega)$. Another contribution for the anticorrelation underlies in the cross term $C_{\rm cross}$ which depends on the $\nu_{IR}\tilde{\Pi}_{IR}$ and $\nu_{RI}\tilde{\Pi}_{RI}$, according to Eq. (5). These terms are interpreted as nonresonant Stokes transitions since they are expressed as the joint products of the kind $\tilde{\Pi}_{IR} = 2\epsilon^2\mathrm{Im}p_2\mathrm{Re}p_1 + \ldots$ ($\tilde{\Pi}_{RI} = 2\epsilon^2\mathrm{Im}p_1\mathrm{Re}p_2 + \ldots$) the absorption in one field $\mathrm{Im}p_2$ ($\mathrm{Im}p_1$) and reemission in the second beam generating the dispersion $\mathrm{Re}p_1$ ($\mathrm{Re}p_2$) for $|\delta| \gtrsim \Gamma$. We can observe that the theoretical C presents a transition from correlation to anticorrelation at that $\delta/2\pi = 5$ MHz determined by the cross term $C_{\rm cross}(\omega)$, which presents the sign inversion at the exact same detuning, as was discussed in Ref. [22]. The asymmetry of such transition point with respect to δ is due to the small one-photon detuning $\Delta = 0.2$ MHz of the fixed beam.

Similar reasoning can be applied to nonresonant cases Figs. 3(a) and 3(c), as we can see in the spectroscopic results

for different one-photon detunings [$\Delta_1/2\pi = -6(1)$ MHz and 5(1) MHz, respectively]. We can start by observing an interesting feature in the change from correlation to anticorrelation at exact resonance of field 2 ($\Delta_2 = 0$ MHz which correspond to $\delta = -\Delta_1$). The understanding is relatively simple. Fluctuations in the frequency (or equivalently their phase diffusion) are common to both beams since they are issued from the same laser. These fluctuations are converted into intensity fluctuations by a variation in the absorption rate of the fields, as the frequencies approach or recede from resonance. Therefore, when the detunings for both beams have the same sign, intensity fluctuations will be correlated. On the other hand, if detunings have opposite sign, the same correlated fluctuation in phase will lead to anticorrelated response of the medium, resulting in anticorrelated fluctuations in intensity. This behavior is closely followed by the cross term C_{cross} since the dispersive component $\tilde{\Pi}_{\text{Re}}$ with the help of the absorptive term is again compensated by the $\chi_{11}(\omega)$ and $\chi_{22}(\omega)$ contributions. Only the contributions of $\tilde{\Pi}_{\text{Im}}$ and $\tilde{\Pi}_{\text{Re}}$, present in the plot of $g^{(2)}(0)$, cannot justify the observed anticorrelation in the frequency domain.

Another curious situation shows up in EIT linewidth, where contribution of dispersion is also reduced and positive compared to the case in Fig. 3(b): anticorrelation is far from saturation in the range of $|\delta|/2\pi = 3 \times \Delta\omega_{\text{EIT}} = 3$ MHz around the EIT condition $\delta = 0$. This structure, carved on the maximized correlation we have just discussed, cannot be completely described only by $g^{(2)}(0)$ since instead of a pair of dips involving a narrow peak, we have also another pair of dips close to the analysis frequency (2 MHz), composing the complete structure of correlation around EIT condition. This case is pretty different from the one-photon resonant case ($\Delta_1 \simeq 0$), seen in Fig. 3(b). The absorptive and dispersive components [$\nu_{\text{Im}}(\omega)\tilde{\Pi}_{\text{Im}}$ and $\nu_{\text{Re}}(\omega)\tilde{\Pi}_{\text{Re}}$] contribute much less than the cross term given by $\nu_{IR}(\omega)\tilde{\Pi}_{IR}$ and $\nu_{RI}(\omega)\tilde{\Pi}_{RI}$, and the individual terms $\chi_{11}(\omega)$ and $\chi_{22}(\omega)$.

Unfortunately, the structures predicted in theory are not so clearly resolved in the experimental results. Therefore, we need a better resolution and a more careful analysis, as we perform next.

A. Resolving the sideband resonances in the correlation spectra

Looking for a better insight into the role of the sidebands of the fields, we show the correlation spectra for different analysis frequencies ω, at the resonant case $\Delta_1 = 0$ in Figs. 4(a)–4(c), and also for detuned case $\Delta_1/2\pi = 6$ MHz in Figs. 4(d)–4(f). In the first row [Figs. 4(a) and 4(d)], we have shown the spectra for $\omega/2\pi = 2$ MHz discussed above. In the second [Figs. 4(b) and 4(e)] and third [Figs. 4(c) and 4(f)] rows, the spectra for $\omega/2\pi = 3$ and 4 MHz are shown, respectively.

The perturbative result of $C(\omega)$ is plotted (dotted-dashed line in Fig. 4) together with the experimental data (solid thick line). The lowest-order term of correlation in ϵ^2 is also plotted in dotted line for $\omega/2\pi = 4$ MHz. In the resonant case $\Delta_1 = 0$ [see Figs. 4(a)–4(c)], there is no spectral independence for the sidebands in the correlation $C(\omega)$ as discussed in Ref. [22]. The intrinsic linewidth of the correlation spectrum [147(9) kHz according to the central peak width] is consistent with the decoherence rate used in the theoretical calculations

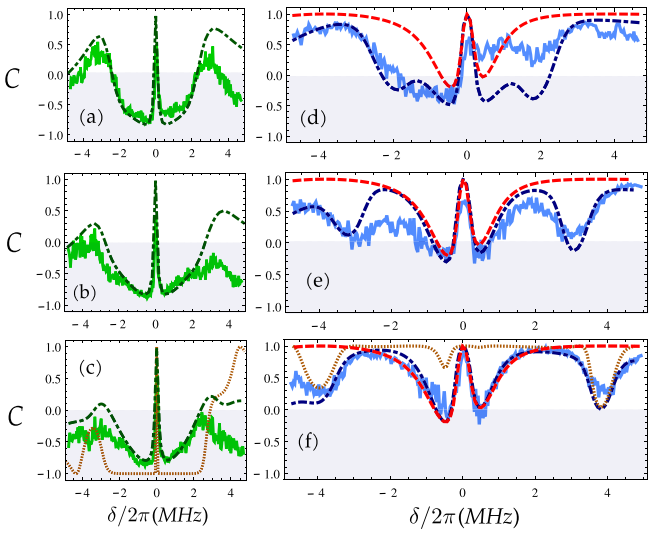

FIG. 4. Correlation spectroscopy for different analysis frequencies ($\omega/2\pi$) with $\Delta_1 = 0$ MHz (first column) and $\Delta_1/2\pi = 6$ MHz (second column). (a), (d) $\omega/2\pi = 2$ MHz, (b), (e) $\omega/2\pi = 3$ MHz, and (c), (f) $\omega/2\pi = 4$ MHz. Experimental correlation $C(\omega)$ is in solid line, theoretical result for $C(\omega)$ is traced with dotted-dashed line, and $g^{(2)}(0)$ is traced with dashed line. In (c), (f) the first-order term of the perturbative model is plotted in dotted line.

(150 kHz). Although the sideband resonance at $\delta \sim -\omega$ seems to be resolved for the first-order term [dotted line, Fig. 4(c)] in the perturbative model, the contribution from higher-order terms suppresses the resolution of sideband resonance. This is due to the fact that near resonance (under the natural linewidth of ~6 MHz), the phase-to-amplitude noise conversion process is dominated by the stimulated and spontaneous emission. Thus, the excess of phase noise is strongly converted into amplitude noise, populating the sidebands with a smoothly varying distribution.

Proceeding now with the nonresonant case ($\Delta_1/2\pi = 6$ MHz) presented in Figs. 4(d)–4(f), we notice that the sideband resonances at $\delta = \pm\omega$ are spectrally resolved once that $\omega > \Delta\omega_{\text{EIT}}$. For $|\delta| < \Delta\omega_{\text{EIT}}$, the intense fields (carriers) determine the correlation profile [Figs. 4(e) and 4(f)]. Thus, the $g^{(2)}(0)$ overlaps with the correlation $C(\omega)$ near the central structure, where carriers are close to the two-photon resonance. The linewidth of the correlation spectra for $C(\omega)$ and $g^2(0)$ are the same (200 kHz). As for the structure in the range $|\delta| > \Delta\omega_{\text{EIT}}$, the reduction of the correlation at $\delta = \pm\omega$ becomes more and more evident for increasing analysis frequencies. The plot of lowest-order term in Fig. 4(f) makes evident this effect, absent for $g^{(2)}(0)$. Since the atomic response to the sideband frequency only depends on the $\nu(\omega)$ coefficients, the correlation at first order (dotted line) does not seem affected by perturbative corrections in the sidebands' resonances, differently from the resonant case shown in Fig. 4(c).

In what follows, we will detail the analysis for the case of $\omega/2\pi = 4$ MHz. At the top of Fig. 5, the correlation spectra of Fig. 4(f) are redrawn. Figure 5(a) shows the main $\tilde{\Pi}$ elements and Figs. 5(b), 5(c), and 5(d) show the $\nu(\omega)$ coefficients that weigh the $\tilde{\Pi}$ elements. Figures 5(c) and 5(d) show the $\nu(\omega)$ coefficients that define the extra term

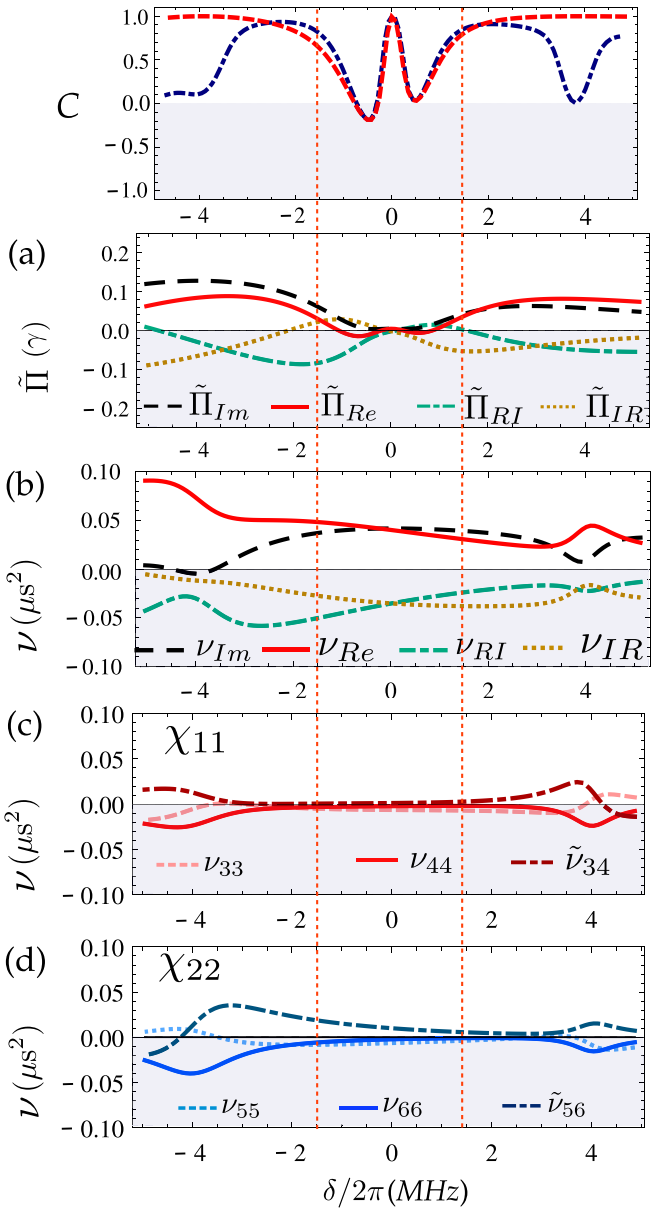

FIG. 5. Mapping between the intensity correlation $C(\omega)$ from Fig. 4(f) and (a) the $\tilde{\Pi}$ elements, (b) the coefficients $\nu_{Im}(\omega)$, $\nu_{\rm Im}(\omega)$, $\nu_{IR}(\omega)$, and $\nu_{RI}(\omega)$ associated to the joint products. In (c) and (d), we plot the $\nu(\omega)$ coefficients associated to extra terms $\chi_{11}(\omega)$ and $\chi_{22}(\omega)$ defined in Eq. (A10). This analysis is done for $\Delta_1/2\pi = 5$ MHz and $\omega/2\pi = 4$ MHz. The two vertical dotted lines indicate the EIT linewidth $\Delta\omega_{\rm EIT}$.

$\chi_{11}(\omega)$ and $\chi_{22}(\omega)$, respectively, from Eq. (A10). Unlike the resonant case in Figs. 3(b) and 4(c) where $\nu_{\rm Im} \ll \nu_{\rm Re}$, in the nonresonant case $\nu_{\rm Im} \sim \nu_{\rm Re}$ for $|\delta|/2\pi < 3$ MHz [see Fig. 5(a)]. Therefore, the absorptive and dispersive response contribute equally to the intensity correlation, while the term $C_{\rm cross}$ [Eq. (6)] nearly cancels due to the opposing behavior of $\tilde{\Pi}_{RI}$ and $\tilde{\Pi}_{IR}$. The residual part from the cross term is canceled by the term $\nu_{56}(\omega)$ in Fig. 5(d). The rest of coefficients $\nu_{ij}(\omega)$ for the extra terms $\chi_{11}(\omega)$ and $\chi_{22}(\omega)$ have almost no contribution to the correlation for $|\delta|/2\pi < 3$ MHz, as it is shown in Figs. 5(c) and 5(d). Therefore, the two main

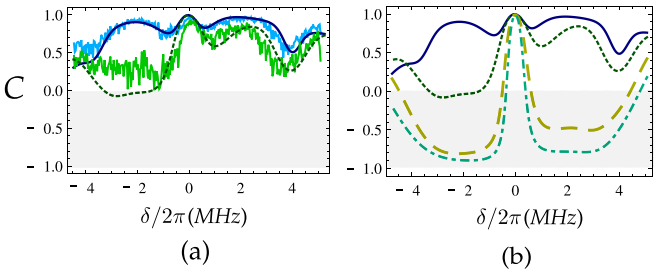

FIG. 6. Correlation spectra for different power of the beams in the nonresonant case $\Delta_1/2\pi = 5$ MHz, at 4 MHz analysis frequency. (a) Experimental correlation spectra for 110 μW (solid line) and 190 μW (dotted line) with their theoretical counterparts. (b) Theoretical results of the correlation spectra (traced with solid lines) for the powers used in (a), and for higher beam powers 3×110 μW (dashed line) and 4×110 μW (dotted-dashed lines).

equal contributions correspond to the absorptive and dispersive which coincides with the heuristic model where the two terms have the same contribution for the $g^{(2)}(0)$ function in Eq. (2). Hence, the two functions describe the same intensity correlation for $|\delta|/2\pi < 3$ MHz in the nonresonant case for higher analysis frequency $\omega > \Delta\omega_{\rm EIT}$.

On the other hand, all the coefficients $\nu(\omega)$ present resonances exactly at the analysis frequency $\delta \sim \pm\omega = \pm(2\pi)$ 4 MHz. The main coefficients $\nu_{\rm Im}(\omega)$ and $\nu_{\rm Re}(\omega)$ present opposite behaviors near the analysis frequency [Fig. 5(a)]. The coefficient $\nu_{\rm Re}$ in solid line shows an increment of the dispersive response while $\nu_{\rm Im}(\omega)$ decreases. However, for the sideband resonance, the contribution of the extra terms associated to $\chi_{11}(\omega)$ and $\chi_{22}(\omega)$ in Figs. 5(c) and 5(d) also compete, leading to $C(\omega) \sim 0$. Curiously, these sideband structures are broad, with nearly half of the width of the EIT peak observed in the dc signal. As we will see, they are also sensitive to power broadening in this case.

B. Power broadening of the resolved sideband structures

We further investigated the correlation spectra for different power of the beams at the nonresonant case. Figure 6(a) shows the correlation spectra for two different powers of the beams. For beam power of 110 μW, i.e., $I/I_{\rm sat} = 0.23$ (solid line), the sideband resonances are well resolved. However, on increasing the power to 190 μW (dotted line) which corresponds to $I/I_{\rm sat} = 0.40$, the resonance at $\delta = -\omega$ near the atomic resonance is sensitive to power broadening.

Further increase in the power leads to a significant push of the atoms during the run of the acquisition. Nevertheless, we can still consider what are the consequences relying on our theoretical model. Figure 6(b) shows the theoretical correlation results for the two cases of power of Fig. 6(a), and also the calculations for higher beam powers 3×110 μW (dashed line) and 4×110 μW (dotted-dashed lines) which correspond to $I/I_{\rm sat} = 0.67$ and $I/I_{\rm sat} = 0.90$, respectively. With increasing power, the central EIT peak broadens and engulfs the sideband structure, now hidden in the anticorrelation flat signal.

IV. DISCUSSION

A linearized approach for the EM field described by Eq. (1) can give useful hints for the mechanisms involved in the spectroscopy studied here. First, we may regard the phase diffusion as a phase modulation process in the limit of small diffusion coefficient γ. When we measure the spectral components of the photocurrent $I(t)$ (generated by an intense, nearly monochromatic field) by their Fourier transform $I(\omega)$, we are in fact investigating the beat notes of the sidebands with the most intense field. For a specific analysis frequency ω the field of interest will involve three components: the carrier at optical frequency ω_i and two sidebands shifted by $\pm\omega$. From Eq. (1) we have the relevant part in calculation of $I(t)$ as

$$\mathbf{E}'_i(t) = \mathcal{E}'(t)_i \exp(i\omega_i t)\mathbf{e}_i, \tag{7}$$

with the complex amplitude given by

$$\mathcal{E}'(t)_i = \mathcal{E}_i + \mathcal{E}_i^u \exp(i\omega t) + \mathcal{E}_i^l \exp(-i\omega t) \tag{8}$$

in a linearized approach for phase diffusion. Pure amplitude modulation will occur if upper and lower sidebands are symmetric and conjugated ($\mathcal{E}_i^u = [\mathcal{E}_i^l]^*$), and pure phase modulation will take place if they are rotated by $\pi/2$ with respect to the carrier amplitude $\mathcal{E}_i$ ($\mathcal{E}_i^u = -[\mathcal{E}_i^l]^*$). Phase and amplitude fluctuations can be converted to each other upon asymmetric shifts of the amplitudes of the sidebands ($\mathcal{E}_i^u$, $\mathcal{E}_i^l$) or by a phase shift of the carrier amplitude $\mathcal{E}_i$ [26]. In our system, the atoms induce such asymmetric shifts in amplitude and phase. Photodetection is sensitive to amplitude modulation, therefore, we observe in our experiment the conversion of random phase modulation (phase noise) into amplitude (intensity) modulation. With that in mind, let us analyze the feature we have observed.

For the case of small single-photon detuning ($\Delta_1 \simeq 0$), the central structure of $C(\omega)$ that we observe at EIT condition ($|\delta| < \Delta\omega_{\mathrm{EIT}}$), which is very similar to the $g^{(2)}(0)$ described in [11], is a consequence of the phase shifts given to the central carriers while we scan the EIT resonance [see Fig. 7(a)]. Those shifts convert phase-to-amplitude noise with opposite signals for fields 1 and 2 (fixed and scanned), leading to a growing anticorrelated response as the intensity is increased, overwhelming the faint intensity correlation that the laser beams may originally present. Only close to EIT resonance (process 1) those initial intensity correlations are recovered since the dispersive contribution goes to zero. Therefore, we have a narrow central peak in the correlation spectroscopy, either in frequency or time domain. In this case, sidebands are nearly unaffected in the process, or symmetrically affected: upper (lower) sidebands of both beams have similar dephasing and attenuation (similar transformations for $\mathcal{E}_1^u$ and $\mathcal{E}_2^u$), leading to correlated contributions. The sideband resonances in the processes 2 and 3 are not resolved due to the stimulated and spontaneous emission since the fields couple the atoms resonantly with detunings no bigger than the natural linewidth $|\delta| \sim \omega < \Gamma$ [see Figs. 4(a)–4(c)].

The resonances of the sidebands will be evident in the case when single-photon detuning is of the order of the atomic linewidth [$|\Delta_1| \simeq \Gamma$, see an example in Fig. 7(b)]. Once again, close to EIT condition (process 1), sidebands of both beams will suffer similar amplitude and phase changes. Strong

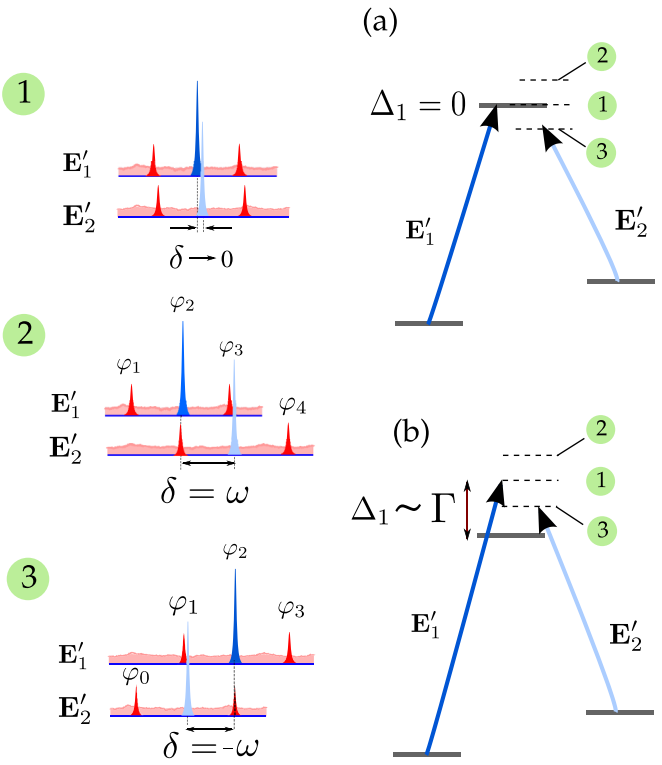

FIG. 7. Description for the correlation spectroscopy. Three main situations of interest are as follows: (process 1) the EIT condition when $\delta \sim 0$, (process 2) when the carrier of the field $\mathbf{E}_2$ is resonant with the upper sideband of the field $\mathbf{E}_1$ ($\delta \sim \omega$), and (process 3) when carrier is resonant with the lower sideband ($\delta \sim -\omega$). These processes can be analyzed for two different cases of one-photon detuning: (a) resonant case $\Delta_1 = 0$, (b) nonresonant case $\Delta_1 \sim \Gamma$.

correlations are then expected, leading to a maximum of the normalized correlation at exact EIT condition ($|\delta| \simeq 0$) for the same reasons presented in the previous case.

The novelty here is the fact that when detuning matches analysis frequency ($|\delta| = \omega$), correlation is reduced. Consider a simple model of phase fluctuations, given in Eq. (8), where $\mathcal{E}_i^u = -[\mathcal{E}_i^l]^* = \alpha$. Phase transformation for the fixed beam will be given by

$$\begin{aligned}\mathcal{E}'(t)_1 &= \alpha e^{i\omega t} + \mathcal{E}_1 - \alpha^* e^{-i\omega t} \to \\ \mathcal{E}'(t)_1 &= \alpha e^{i(\omega t+\varphi_3)} + \mathcal{E}_1 e^{i\varphi_2} - \alpha_1^* e^{-i(\omega t-\varphi_1)} \\ &= \left[\alpha e^{i(\omega t+\varphi_3-\varphi_2)} + \mathcal{E}_1 - \alpha^* e^{-i(\omega t+\varphi_2-\varphi_1)}\right] e^{i\varphi_2}. \end{aligned} \tag{9}$$

Therefore, different phase shifts will convert phase to amplitude fluctuations.

Applying the same transformation for the second field when its carrier is resonant with the upper band of the fixed field (process 2),

$$\begin{aligned}\mathcal{E}'(t)_2 &= \alpha e^{i\omega t} + \mathcal{E}_2 - \alpha^* e^{-i\omega t} \to \\ \mathcal{E}'(t)_2 &= \alpha e^{i(\omega t+\varphi_4)} + \mathcal{E}_2 e^{i\varphi_3} - \alpha^* e^{-i(\omega t-\varphi_2)} \\ &= \left[\alpha e^{i(\omega t+\varphi_4-\varphi_3)} + \mathcal{E}_2 - \alpha^* e^{-i(\omega t+\varphi_3-\varphi_2)}\right] e^{i\varphi_3}. \end{aligned} \tag{10}$$

Notice that when we discard the overall phase (unobserved upon intensity detection), the effective shift of the upper band of field 1 is the conjugate of the phase shift of the lower

sideband of field 2. Fluctuations will rotate in opposite directions in a Fresnel diagram, and resulting intensity correlations will be anticorrelated.

Now, if the carrier of the second field is resonant with the lower band of the fixed field (process 3), transformation will be given by

$$\begin{aligned}\mathcal{E}'(t)_2 &= \alpha e^{i\omega t} + \mathcal{E}_2 - \alpha^* e^{-i\omega t} \rightarrow \\ \mathcal{E}'(t)_2 &= \alpha e^{i(\omega t+\varphi_2)} + \mathcal{E}_2 e^{i\varphi_1} - \alpha^* e^{-i(\omega t-\varphi_0)} \\ &= \left[\alpha e^{i(\omega t+\varphi_2-\varphi_1)} + \mathcal{E}_2 - \alpha^* e^{-i(\omega t+\varphi_1-\varphi_0)}\right] e^{i\varphi_1}. \end{aligned} \quad (11)$$

The phase shift of the upper sideband of field 2 will be the conjugate of the phase shift of the upper sideband of field 1. Once again, anticorrelation will contribute to the result of $C(\omega)$.

This conversion depends on the phase gained by each mode. Under power broadening of the EIT resonance [11,12], anticorrelation will be affected by the reduction on the difference of phase shifts, as is the case in Fig. 6.

V. CONCLUSIONS

Correlation spectroscopy for two light fields interacting with cold-atomic medium at different one-photon detunings has been explored. When the one-photon detuning is of the order of the natural linewidth and beam intensities are much smaller than the saturation limit, the correlation spectroscopy presents resonances at the sidebands frequency. If the analysis frequency is larger than the typical EIT linewidth, the intensity correlation spectra in the EIT range can be approximately described by the $g^{(2)}(0)$ function [11]. Therefore, the intrinsic linewidth measured with the $g^{(2)}(0)$ function in time domain corresponds exactly to the one observed with the correlation spectrum $C(\omega)$ in frequency domain.

Sideband resonances are auxiliary spectroscopic tools for the study of the EIT process, and can be resolved for analysis frequencies higher than the EIT linewidth. However, in such a condition, the sideband resonances are sensitive to power broadening. It was also shown that for fields close to atomic resonance, the contributions from the sidebands and the carriers are mixed, disabling any spectral independence of sidebands in the correlation spectroscopy. The resolution of the sideband resonances is only possible with the use of cold atoms. The next step is to measure correlation spectra using a coherent source to verify if it is possible to measure a narrower intrinsic linewidth for resonant conditions as it is predicted by the first-order term in the perturbative model [22].

ACKNOWLEDGMENTS

This work was supported by Grants No. 2004/13587-0 and No. 2010/08448-2, São Paulo Research Foundation (FAPESP), CNPq and CAPES (Brazilian agencies), and INCT-IQ (Instituto Nacional de Ciência e Tecnologia de Informação Quântica). The authors would like to thank Professor Dr. V. S. Bagnato and Dr. K. M. F. Magalhães, from IFSC-USP, for gently providing the Rb for our MOT.

APPENDIX: SOLUTION FOR NOISE SPECTRA

The intensity correlation result in Eq. (5) is demonstrated in detail in Ref. [22]. Shortly, to describe the role of the atomic response in the PN-AN conversion, we should begin by writing the density matrix elements $\mathbf{x} = (\rho_{11},\rho_{22},\rho_{13},\rho_{31},\rho_{23},\rho_{32},\rho_{12},\rho_{21})$. It can be expanded on the ϵ parameter, that we will eventually associate with the laser linewidth,

$$\mathbf{x}(t) = \mathbf{x}^{(0)}(t) + \epsilon\, \mathbf{x}^{(1)}(t) + \epsilon^2 \mathbf{x}^{(2)}(t) + \dots . \quad (A1)$$

The stationary state of the zero-order terms is defined as $\langle \mathbf{x}_{ss}^{(0)} \rangle = (\rho_{11}^{(0)},\rho_{22}^{(0)},p_1,p_1^*,p_2,p_2^*,,\rho_{12}^{(0)},\rho_{21}^{(0)})$. Its stationary solution is $\langle \mathbf{x}_{ss}^{(0)} \rangle = \mathbf{M}^{-1}\mathbf{x}_o$ with $\mathbf{x}_o$ as a constant vector and the $\mathbf{M}$ matrix contains all the parameters of the atom-light interaction.

The covariances between the atomic density matrix elements are also expanded as

$$\Pi = \epsilon^2 \sigma^{(0)} + \sum_{n=2}^{\infty} \epsilon^{2n} \sigma^{(2n-2)}, \quad (A2)$$

where $\Pi_{ij} = \langle \mathbf{x}_i(t), \mathbf{x}_j(t)^\dagger \rangle$ and $\sigma_{ij} = \langle \mathbf{x}_i^{(n)}(t), \mathbf{x}_j^{(n)}(t)^\dagger \rangle$. The stationary solution for the zero-order term is defined as

$$\sigma_{ss}^{(0)} = (\mathbf{M})^{-1} \mathbf{x}_o \mathbf{x}_o^\dagger (\mathbf{M}^\dagger)^{-1} \quad (A3)$$

and higher-order terms satisfy

$$\mathbf{M}\sigma_{ss}^{(2n)} + \sigma_{ss}^{(2n)}\mathbf{M}^\dagger = 2\ \Phi\ \sigma_{ss}^{2(n-1)}\ \Phi^\dagger, \qquad n \geqslant 1 \quad (A4a)$$

$$\sigma_{ss}^{(2n-1)} = 0, \qquad n \geqslant 2. \quad (A4b)$$

It is useful to transform the atomic vector as $\tilde{\mathbf{x}}(t) = \mathbf{U}\,\mathbf{x}(t)$ where $\mathbf{U}$ converts $x_i(t)$ for $i = \{3\text{–}6\}$ into their real and imaginary parts. Therefore, the covariances Π and σ^n will transform also according to $\mathbf{U}$ as $\tilde{\Pi}$ and $\tilde{\sigma}^{(n)}$.

The noise spectra S_{11} and S_{22} in Eq. (5) are given by

$$\begin{aligned} S_{11}(\omega) = {} & \alpha_{33}(\omega)\left[2\epsilon^2 \mathrm{Im}^2 p_1 + \sum_{n=2}^{\infty} \epsilon^{2n} \tilde{\sigma}_{33}^{(2n-2)}\right] \\ & + \alpha_{44}(\omega)\left[2\epsilon^2 \mathrm{Re}^2 p_1 + \sum_{n=2}^{\infty} \epsilon^{2n} \tilde{\sigma}_{44}^{(2n-2)}\right] \\ & + \tilde{\alpha}_{34}(\omega)\left[-2\epsilon^2 \mathrm{Im} p_1 \mathrm{Re} p_1 + \sum_{n=2}^{\infty} \epsilon^{2n} \tilde{\sigma}_{34}^{(2n-2)}\right] \\ & + C_{11}(\omega) \end{aligned} \quad (A5)$$

and

$$\begin{aligned} S_{22}(\omega) = {} & \beta_{55}(\omega)\left[2\epsilon^2 \mathrm{Im}^2 p_2 + \sum_{n=2}^{\infty} \epsilon^{2n} \tilde{\sigma}_{55}^{(2n-2)}\right] \\ & + \beta_{66}(\omega)\left[2\epsilon^2 \mathrm{Re}^2 p_2 + \sum_{n=2}^{\infty} \epsilon^{2n} \tilde{\sigma}_{66}^{(2n-2)}\right] \\ & + \tilde{\beta}_{56}(\omega)\left[-2\epsilon^2 \mathrm{Im} p_2 \mathrm{Re} p_2 + \sum_{n=2}^{\infty} \epsilon^{2n} \tilde{\sigma}_{56}^{(2n-2)}\right] \\ & + C_{22}(\omega), \end{aligned} \quad (A6)$$

where $\tilde{X}_{ij}(\omega) = X_{ij}(\omega) + X_{ji}(\omega)$ with $X = \alpha$, β, and ν. The products $\mathrm{Im}p_i\mathrm{Im}p_j$, $\mathrm{Re}p_i\mathrm{Re}p_j$, and $\mathrm{Im}p_i\mathrm{Re}p_j$ are associated to the elements $\sigma^{(0)}_{i+2,j+2}$ with $i,j = 1,2$. The additional $C_{11}(\omega)$ and $C_{22}(\omega)$ terms are defined as

$$\begin{aligned} C_{11}(\omega) = {} & \alpha_{55}(\omega)\tilde{\Pi}_{55} + \alpha_{66}(\omega)\tilde{\Pi}_{66} + \tilde{\alpha}_{56}(\omega)\tilde{\Pi}_{56} \\ & + \tilde{\alpha}_{35}(\omega)\tilde{\Pi}_{35} + \tilde{\alpha}_{46}(\omega)\tilde{\Pi}_{46} \\ & + \tilde{\alpha}_{36}(\omega)\tilde{\Pi}_{36} + \tilde{\alpha}_{45}(\omega)\tilde{\Pi}_{45} \end{aligned} \tag{A7}$$

and

$$\begin{aligned} C_{22}(\omega) = {} & \beta_{33}(\omega)\tilde{\Pi}_{33} + \beta_{44}(\omega)\tilde{\Pi}_{44} + \tilde{\beta}_{34}(\omega)\tilde{\Pi}_{34} \\ & + \tilde{\beta}_{35}(\omega)\tilde{\Pi}_{35} + \tilde{\beta}_{46}(\omega)\tilde{\Pi}_{46} \\ & + \tilde{\beta}_{36}(\omega)\tilde{\Pi}_{36} + \tilde{\beta}_{45}(\omega)\tilde{\Pi}_{45}, \end{aligned} \tag{A8}$$

respectively.

The cross product that defines the intensity correlation in Eq. (5) is given by

$$\begin{aligned} S_{12}(\omega) = {} & \nu_{\mathrm{Im}}(\omega)\left[2\epsilon^2\mathrm{Im}p_1\mathrm{Im}p_2 + \sum_{n=2}^{\infty}\epsilon^{2n}\tilde{\sigma}^{(2n-2)}_{35}\right] \\ & + \nu_{\mathrm{Re}}(\omega)\left[2\epsilon^2\mathrm{Re}p_1\mathrm{Re}p_2 + \sum_{n=2}^{\infty}\epsilon^{2n}\tilde{\sigma}^{(2n-2)}_{46}\right] \\ & + \nu_{RI}(\omega)\left[-2\epsilon^2\mathrm{Im}p_1\mathrm{Re}p_2 + \sum_{n=2}^{\infty}\epsilon^{2n}\tilde{\sigma}^{(2n-2)}_{36}\right] \\ & + \nu_{IR}(\omega)\left[-2\epsilon^2\mathrm{Im}p_2\mathrm{Re}p_1 + \sum_{n=2}^{\infty}\epsilon^{2n}\tilde{\sigma}^{(2n-2)}_{45}\right] \\ & + C_{1|2}, \end{aligned} \tag{A9}$$

where $C_{1|2}$ is given by

$$C_{1|2} = \chi_{11}(\omega) + \chi_{22}(\omega) \tag{A10}$$

with $\chi_{11}(\omega)$ and $\chi_{22}(\omega)$ defined as

$$\begin{aligned} \chi_{11} &= \nu_{33}(\omega)\tilde{\Pi}_{33} + \nu_{44}(\omega)\tilde{\Pi}_{44} + \tilde{\nu}_{34}(\omega)\tilde{\Pi}_{34}, \\ \chi_{22} &= \nu_{55}(\omega)\tilde{\Pi}_{55} + \nu_{66}(\omega)\tilde{\Pi}_{66} + \tilde{\nu}_{56}(\omega)\tilde{\Pi}_{56}. \end{aligned} \tag{A11}$$

[1] S. E. Harris, Phys. Today **50**(7), 36 (1997).
[2] K. J. Boller, A. Imamoglu, and S. E. Harris, Phys. Rev. Lett. **66**, 2593 (1991).
[3] A. Imamoglu, M. Fleischhauer, and J. P. Marangos, Rev. Mod. Phys. **77**, 633 (2005).
[4] L.-M. Duan, M. D. Lukin, J. I. Cirac, and P. Zoller, Nature (London) **414**, 413 (2001).
[5] M. D. Lukin, Rev. Mod. Phys. **75**, 457 (2003).
[6] K. Hammerer, A. S. Sørensen, and E. S. Polzik, Rev. Mod. Phys. **82**, 1041 (2010).
[7] J.-F. Roch, K. Vigneron, Ph. Grelu, A. Sinatra, J.-Ph. Poizat, and Ph. Grangier, Phys. Rev. Lett. **78**, 634 (1997).
[8] A. Dantan, J. Cviklinski, E. Giacobino, and M. Pinard, Phys. Rev. Lett. **97**, 023605 (2006).
[9] C. Garrido-Alzar, L. S. Cruz, J. G. Aguirre-Gómez, M. F. Santos, and P. Nussenzveig, Europhys. Lett. **61**, 485 (2003).
[10] Y. Xiao, T. Wang, M. Baryakhtar, M. Van Camp, M. Crescimanno, M. Hohensee, L. Jiang, D. F. Phillips, M. D. Lukin, S. F. Yelin, and R. L. Walsworth, Phys. Rev. A **80**, 041805 (2009).
[11] D. Felinto, L. S. Cruz, R. A. de Oliveira, H. M. Florez, M. H. G. de Miranda, P. Nussenzveig, M. Martinelli, and J. W. R. Tabosa, Opt. Express **21**, 1512 (2013).
[12] H. M. Florez, L. S. Cruz, M. H. G. de Miranda, R. A. de Oliveira, J. W. R. Tabosa, M. Martinelli, and D. Felinto, Phys. Rev. A **88**, 033812 (2013).
[13] J. Vanier, Appl. Phys. B **81**, 421 (2005).
[14] T. Yabuzaki, T. Mitsui, and U. Tanaka, Phys. Rev. Lett. **67**, 2453 (1991).
[15] V. A. Sautenkov, Y. V. Rostovtsev, and M. O. Scully, Phys. Rev. A **72**, 065801 (2005).
[16] G. A. Ariunbold, Y. V. Rostovtsev, V. A. Sautenkov, and M. O. Scully, J. Mod. Opt. **57**, 1417 (2010).
[17] H. Li, V. A. Sautenkov, T. S. Varzhapetyan, Y. V. Rostovtsev, and M. O. Scully, J. Opt. Soc. Am. B **25**, 1702 (2008).
[18] M. Martinelli, P. Valente, H. Failache, D. Felinto, L. S. Cruz, P. Nussenzveig, and A. Lezama, Phys. Rev. A **69**, 043809 (2004).
[19] L. S. Cruz, D. Felinto, J. G. Aguirre Gómez, M. Martinelli, P. Valente, A. Lezama, and P. Nussenzveig, J. Eur. Phys. D **41**, 531 (2007).
[20] O. Pinel, P. Jian, R. M. de Araujo, J. Feng, B. Chalopin, C. Fabre, and N. Treps, Phys. Rev. Lett. **108**, 083601 (2012).
[21] G. Campbell, A. Ordog, and A. I. Lvovsky, New J. Phys. **11**, 103021 (2009).
[22] H. M. Florez, C. González, and M. Martinelli, this issue, Phys. Rev. A **94**, 012503 (2016).
[23] L. Feng, P. Li, M. Zhang, T. Wang, and Y. Xiao, Phys. Rev. A **89**, 013815 (2014).
[24] R. Walser and P. Zoller, Phys. Rev. A **49**, 5067 (1994).
[25] A. Lezama, S. Barreiro, and A. M. Akulshin, Phys. Rev. A **59**, 4732 (1999).
[26] A. S. Villar, Am. J. Phys. **76**, 922 (2008).